Low-temperature interface reactions in layered Au/Sb films: *In situ* investigation of the formation of an amorphous phase

H.-G. Boyen, A. Cossy-Favre, and P. Oelhafen
Institut für Physik, Universität Basel, Klingelbergstrasse 82, Ch-4056 Basel, Switzerland

A. Siber and P. Ziemann
Fakultät für Physik, Universität Konstanz, P.O. Box 5560, D-78434 Konstanz, Germany

C. Lauinger,* T. Moser, P. Häussler,* and F. Baumann
Physikalisches Institut, Universität Karlsruhe, Engesserstrasse 7, D-76128 Karlsruhe, Germany
(Received 6 September 1994)

Photoelectron-spectroscopy methods combined with electrical-resistance measurements were employed to study the effects of intermixing at Au/Sb interfaces at low temperatures. For the purpose of characterizing the growth processes of the intermixed phase on a ML scale, Au/Sb bilayers (layer thicknesses $D_{Au}=0.5-75$ ML and $D_{Sb}=150$ ML) were evaporated at 77 K and the different *in situ* techniques allowed a comparison to vapor-quenched amorphous Au_xSb_{100-x} alloys. For Au thicknesses between 0.5 and 0.9 ML, a change from a semiconducting to a metallic behavior of the samples has been detected, as indicated by the development of a steplike photoelectron intensity at the Fermi level. Evidence has been found that for Au coverages $\leq$ 6 ML chemical reactions at the Au/Sb interface occur, leading to the formation of a homogeneously intermixed amorphous layer with a maximum thickness of about 2.3 nm and Au concentrations as high as $x \approx 80$ at. %. This latter value corresponds to the limiting Au content where amorphous alloys can be prepared at low temperature (0 at. % $\leq x \leq$ 80 at. %). For nominal coverages beyond 6 ML polycrystalline Au films were formed. Consequently, Au/Sb multilayers with sufficiently small modulation lengths, which were prepared at 130 K by ion-beam sputtering, were observed to grow as a homogeneous amorphous phase over a broad range of compositions, as evidenced by *in situ* resistance measurements and by comparing the obtained crystallization temperatures to those of vapor-quenched amorphous alloys. Variation of the deposition temperature T_s revealed that an amorphous interface layer is only formed for $T_s \leq 220$ K. This is consistent with the fact that for multilayers with large modulation lengths containing unreacted polycrystalline Au and Sb layers, long-range interdiffusion is found to set in at temperatures above 230 K. This interdiffusion, however, results in the formation of polycrystalline Au-Sb alloys.

I. INTRODUCTION

Within modern solid-state physics, systems with reduced dimensions have attracted much attention not only because of their relevance to technical applications such as, e.g., in microelectronics, but also from a fundamental point of view. Important new insights into quantum-mechanical phenomena have been found in systems whose physical dimensions could be strongly reduced such as, e.g., in mesoscopic systems or extremely thin films. With advances in thin-film preparation techniques and the availability of sophisticated sample characterization tools, it has become possible to fabricate and analyze ultrathin structures with a degree of interfacial smoothness on the atomic scale. Thin films, bilayers, and multilayers with compositional modulation lengths of several angstroms have been widely used to study phenomena such as superconductivity,[1-3] magnetism,[4,5] localization–electron-electron interaction,[6-8] and quantum-size effects,[9-11] to give just a few examples.

In multilayered systems, much work has been motivated by the idea that coupling between different layers may result in new and fascinating properties which can be significantly different from those of each of the components. Such a coupling can either be mediated by conduction electrons[5,7] or emerge from reactions between different types of atoms at interfaces.[1] Since interface effects usually penetrate at least a few atomic layers into the bulk, in layered systems with very short modulation lengths the existence of reacted interface layers seems to offer the possibility to design macroscopic samples with properties dominated by the microscopic structure of the interfacial region. This structure can range from being perfectly ordered for epitaxial layer growth to completely disordered (amorphous) interface alloys at sufficient low temperatures in systems showing strong tendencies for intermixing.

The aim of the present work is to establish the nature of the electronic states which develop at the interface between two different types of materials, in our case Au and Sb. Because of the large negative heat of formation of the AuX_2 compounds (X = In, Al, Ga, Sb, etc.), one might expect that Au atoms, rather than acting as an inert noble metal, may chemically react with the polyvalent Sb atoms to form either a crystalline compound ($AuSb_2$) or, at sufficient low temperature, an amorphous phase whose

 ©1995 The American Physical Society

existence is well known from earlier experiments.[12] Recently, metallic multilayers of Au/In (Ref. 13) and Au/Al (Ref. 14) with very small individual layer thicknesses were found to be completely amorphized by strong chemical reactions even at 85 K. This new method has proved to be different from the thermally driven solid-state amorphization,[15,16] a technique which sometimes allows the amorphization of crystalline multilayered systems by thermally activated fast diffusion of one of the components into the other. Also in this case, when thick layers can be forced into the disordered state by thermally activated solid-state reactions, ultrathin amorphous interface layers have been reported to form in the as-deposited state without applying an additional heat treatment,[17–19] indicating that amorphization at interfaces is a very general phenomenon. This new additional route into the metastable amorphous state has been investigated by means of different analytical tools such as electrical resistance measurements,[13,14,20] the perturbed $\gamma\gamma$-angular correlation technique,[20] Auger electron spectroscopy, and electron-energy-loss spectroscopy.[21,22] Unfortunately, all these methods cannot be used to extract a direct picture of the electronic states during the growth of the reacted phase. Further experiments would be valuable in allowing us to distinguish directly whether an amorphous or a crystalline phase is formed.

Because of its inherent surface sensitivity (2–10 ML) combined with high-energy resolution, ultraviolet and monochromatized x-ray photoelectron spectroscopy (UPS and MXPS) have been applied in the present work to establish a direct picture of the electronic states which will be created at the interfacial region during the stepwise deposition of Au atoms on top of a thick Sb layer at 77 K. While the UPS technique is used to analyze details of the valence-band structure of the reacted phase, core-level spectroscopy gives additional information on the chemical reaction between the two types of atoms. Since resistivity measurements are also sensitive to the density of states near the Fermi energy E_F, it is of particular interest to combine all three methods in order to investigate the electronic structure of the interface layer. It will be demonstrated that these methods are well suited to extract direct information on the formation of an amorphous (in the present case metallic) interface layer and its limiting thickness. In addition, resistivity measurements on various Au/Sb multilayers will show that the Au/Sb system represents a further example where interface reactions can be exploited to prepare thick amorphous samples over a broad range of compositions. These measurements will also confirm that thermally activated solid-state reactions can be excluded to be responsible for the formation of the disordered alloy at low temperatures.

II. EXPERIMENT

The photoemission experiments on Au/Sb bilayers were performed in a Leybold-Heraeus EA11-100 electron spectrometer consisting of a preparation chamber equipped with two electron-beam evaporators and an analysis chamber where photoelectrons can be recorded by means of a hemispherical energy analyzer. Samples were prepared by quench condensation of thick Sb films ($D_{Sb}=150$ ML) onto fused-quartz substrates kept at 77 K, followed by the stepwise evaporation of Au on top of the Sb surface up to a total coverage of 75 ML. The electron-beam evaporators were adjusted to give deposition rates of typically 0.01 ML/sec (Au) and 0.1 ML/sec (Sb), both rates controlled by means of quartz-crystal monitors. All evaporation processes were performed at a pressure less than 5×10^{-9} mbar.

After each evaporation step the samples were transferred into the analysis chamber where the photoelectron spectroscopy methods have been applied at a base pressure less than 10^{-10} mbar. During this whole procedure, the samples were kept at the deposition temperature $T_s=77$ K. An UPS resonance discharge lamp (He I, $h\nu=21.2$ eV) was used to investigate the valence-band structure, monochromatized x rays (Al $K\alpha$, $h\nu=1486.6$ eV) to characterize core levels for chemical analysis. Whereas no indications have been found for the existence of any contaminations in the as-prepared state, a small amount of oxygen could be detected after several hours at 77 K reflecting the condensation of residual gas atoms onto the samples. All spectra have been recorded in the pass energy mode, giving a constant energy resolution of 60 meV and 0.6 eV (full width at half maximum) for the UPS and MXPS measurements, respectively. No additional data processing such as background subtraction or satellite correction (UPS) has been applied.

The Au/Sb multilayers (individual layer thickness of Au, 0.42 nm, and Sb, 1.5 nm) were deposited at 130 K $\leq T_s \leq$ 250 K by means of ion-beam sputtering of elemental Au and Sb targets using 0.5-keV Ar^+ ions from a Kaufman-type ion source within an UHV chamber (residual gas pressure prior to sputtering 3×10^{-9} mbar, Ar partial pressure during sputtering 7×10^{-5} mbar). The sputtered atoms were collected on fused-quartz substrates whose temperature could be controlled between 100 and 390 K. Typical growth rates of the layers were 0.03 nm/sec. During deposition the resistance of the growing multilayers was monitored applying the standard four-probe technique using pre-evaporated Ag contacts. Further details of the experimental setup are given in Ref. 23. After the deposition of typically 20 Au/Sb bilayers each multilayer was annealed *in situ* up to 390 K, simultaneously monitoring its resistance. In this way, structural changes, which are reflected in the resistance behavior such as crystallization from an amorphous phase or interdiffusion and formation of a polycrystalline alloy, can be detected.

III. RESULTS AND DISCUSSION

A. Valence-band spectroscopy on Au/Sb bilayers

One aim of this work was to establish how valence-band states will develop after the deposition of Au atoms onto a clean Sb surface at low temperatures. In Fig. 1 valence-band spectra are shown for Au overlayer thicknesses up to 1.3 ML. The lowest curve corresponds to freshly prepared Sb, which is a disordered semiconductor at 77 K. Based on the fact that, in disordered materi-

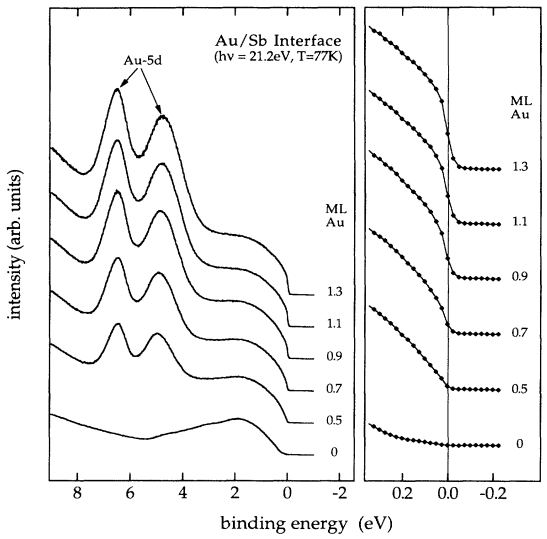

FIG. 1. Valence-band spectra of the Au/Sb interfacial region measured at a photon energy of 21.2 eV (UPS, He I) for Au coverages up to 1.3 ML. The binding energy is referred to the Fermi level E_F. The two peaks observed at binding energies of about 5 and 6.5 eV, respectively, reflect the Au $5d$ contribution to the valence band.

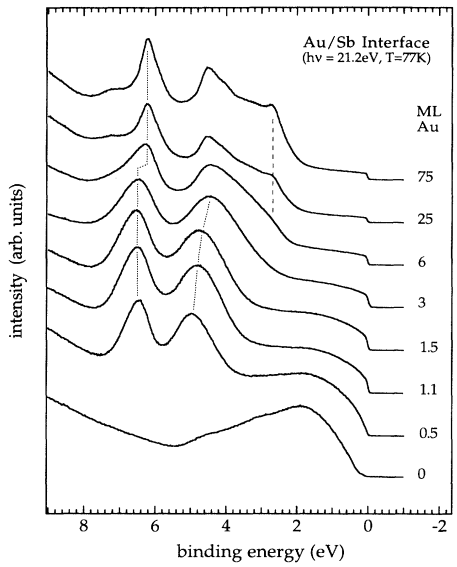

FIG. 2. UPS spectra ($h\nu=21.2$ eV) of the Au/Sb overlayer system for Au coverages up to 75 ML.

als, photoemission intensities represent the sum of different partial densities of states weighted by the corresponding photoionization cross sections, only the p part of the Sb valence-band structure is visible at a photon energy of $h\nu=21.2$ eV, while the s part appears to be strongly suppressed. This is due to a Sb $5s$ photoionization cross section which, in the atomic limit, is about two orders of magnitude smaller than the corresponding value for Sb $5p$ states.[24] The p part of the Sb valence band extends in the binding-energy range between $E_b=0$ and 5.5 eV, sitting on a background of secondary electrons which increases to higher binding energies. After adding 0.5 ML of Au two nearly symmetric peaks can be recognized, representing the Au $5d_{3/2}$ and $5d_{5/2}$ bands centered at $E_b\approx 6.5$ and 5.0 eV, respectively. By increasing the thickness of the Au overlayer an enhanced emission from the Au $5d$ band is detected, accompanied by a rising photoelectron intensity near the Fermi energy E_F. The binding-energy range near E_F has been displayed on an enlarged scale on the right-hand side of Fig. 1. For an Au coverage of approximately 0.5–0.9 ML, a steplike electron distribution curve (EDC) develops, which is smeared out by the resolution function of the energy analyzer. This provides strong evidence that a semiconductor-to-metal transition occurs for an Au overlayer thickness in the submonolayer range.

In Fig. 2 the valence-band spectra of the interface layer have been plotted for overlayer thicknesses D_{Au} up to 75 ML. Again systematic trends in the development of the curve shape can be recognized: while the Au $5d_{3/2}$ band position remains unchanged for Au coverages up to 3 ML, a distinct shift to lower binding energies occurs for $D_{\mathrm{Au}}\geq 6$ ML, which is correlated with the appearance of an additional shoulder at $E_b=7.3$ eV. At the same time the Au $5d_{5/2}$ band, which exhibits a symmetric band shape for overlayer thickness less than or equal to 3 ML, shifts to lower binding energies. For $D_{\mathrm{Au}}=6$ ML, this symmetric band shape is slightly changed due to an additional shoulder at $E_b=2.7$ eV, resulting in a distinct peak for higher Au coverages (vertical dashed line). Therefore the EDC corresponding to $D_{\mathrm{Au}}=6$ ML seems to separate two groups of curves which, in the following, will be identified as being due to amorphous ($D_{\mathrm{Au}}<6$ ML) and polycrystalline ($D_{\mathrm{Au}}>6$ ML) material, respectively.

These photoemission results will now be compared with data taken in previous studies on vapor-quenched $\mathrm{Au}_x\mathrm{Sb}_{100-x}$ alloys,[25] which can be prepared in the amorphous state over a broad range of compositions (0 at. $\%\leq x\leq 80$ at. %). In Fig. 3 EDC's of amorphous $\mathrm{Au}_x\mathrm{Sb}_{100-x}$ alloys are displayed as a function of the Au content x (solid lines). Valence-band data of polycrystalline alloys and of an Au reference sample (dotted lines) have been added. By analyzing the details of the band shape as a function of the composition, similar tendencies can be recognized as in the case of Fig. 2. For rising Au concentration x, the Au $5d_{3/2}$ band position remains stable for x values less than 80 at. % and moves slightly toward the Fermi energy for higher values where an additional shoulder shows up at a binding energy $E_b=7.3$ eV. Again the Au $5d_{5/2}$ band, which is symmetric for the amorphous alloys, shifts toward lower binding energies and significantly changes its shape after the transition into the polycrystalline phase because of an enhanced intensity at $E_b=2.7$ eV.

These close similarities clearly suggest that Au atoms deposited at 77 K on top of Sb will be chemisorbed, leading to an intermixed layer with *disordered* structure for Au coverages up to 6 ML. At an overlayer thickness of 6

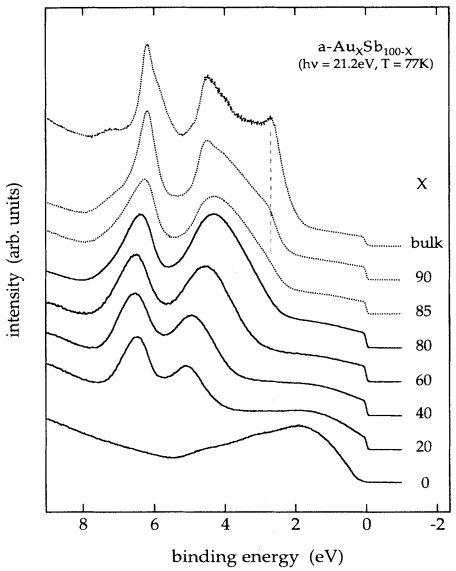

FIG. 3. Valence-band spectra ($h\nu$=21.2 eV) of *in situ* prepared Au_xSb_{100-x} alloys (Ref. 25). The alloys are observed to grow as a homogeneous amorphous phase for Au concentrations $x \leq 80$ (solid lines).

ML, first indications for a slight admixture of a second (crystalline) phase become evident. In this case the interface layer, having an electronic structure similar to $Au_{85}Sb_{15}$, must be regarded as being mainly amorphous, but no longer consisting of a single phase. In order to corroborate these findings, EDC's of the Au_xSb_{100-x} alloys are shown in Fig. 4, which have been acquired at 477 K, i.e., well above the crystallization temperatures of the amorphous samples.[12,26] Distinct structures can now be recognized that are absent in the amorphous state and

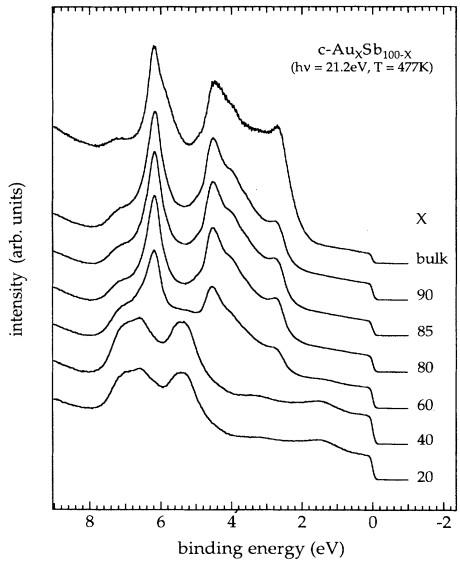

FIG. 4. UPS spectra ($h\nu$=21.2 eV) of Au_xSb_{100-x} alloys measured in the crystalline state.

are partly due to direct transitions of the photoelectrons into unoccupied states. These structures are not present in Fig. 2, corroborating that the intermixing processes at 77 K result in an amorphous rather than a crystalline phase for sufficiently small Au overlayer thicknesses.

The systematic shift of the Au $5d_{5/2}$ band maximum, which has been found for the reacted layer and similarly for the amorphous Au_xSb_{100-x} alloys, can now be used to extract some more details about the growth of the intermixed phase. Such a behavior has been observed in the valence-band structure of a large number of disordered alloys containing Au and a polyvalent element.[25] Together with the stable position of the corresponding Au $5d_{3/2}$ band, this shift toward the Fermi energy reflects an increase in the total Au $5d$ bandwidth due to an increasing number of overlapping Au $5d$ wave functions, equivalent to an increasing Au-Au coordination number in the neighborhood of each Au atom. Therefore the position of the Au $5d_{5/2}$ band maximum can be used as an indication for a certain Au concentration in the system under consideration. In Fig. 5 the binding energies of the Au $5d_{5/2}$ band maximum taken from the Figs. 2 (Au on top of Sb) and 3 (amorphous Au_xSb_{100-x} alloys) are presented as a function of the Au overlayer thickness D_{Au} (lower scale, dots) and the Au concentration x (upper scale, squares). Solid lines have been added as a guide to the eye. Obviously the deposition of an increasing number of Au atoms onto Sb leads to a monotonic decrease of the binding energy of the Au $5d_{5/2}$ band maximum, thereby indicating an increasing Au content of the amorphous interlayer. By relating the UPS binding-energy shifts of both systems, a rough estimate of the average Au concentration of the intermixed layer can be obtained, leading to approximate values for the thickness of the reacted Sb layer. The resulting data are shown in Fig. 6. At very low coverages, the Au atoms seem to mix with Sb atoms mainly located within the top layer of the substrate film (left scale, dots) to form an amorphous al-

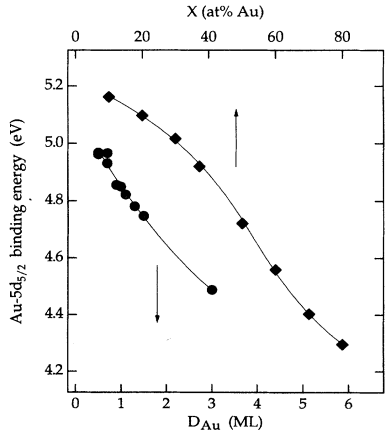

FIG. 5. Binding-energy values of the Au $5d_{5/2}$ valence-band maximum plotted as function of the Au overlayer thickness D_{Au} (bottom axis, dots) and the Au concentration of the amorphous alloys x (top axis, squares), respectively. Solid lines have been added as a guide to the eye.

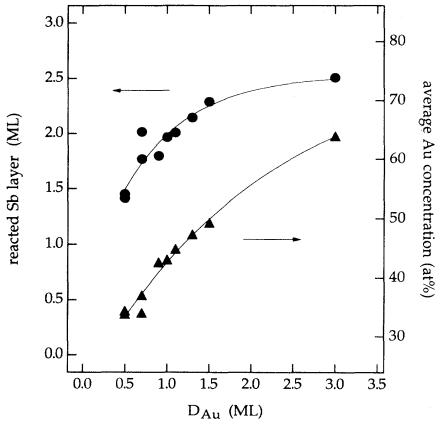

FIG. 6. Estimated values for the average Au concentration of the intermixed phase (right scale, triangles) and the Sb contribution to the reacted layer (left scale, dots) as function of the Au overlayer thickness D_{Au}.

loy of composition $Au_{34}Sb_{66}$ (right scale, triangles). For rising D_{Au} the amorphous intermixed layer slightly extends into the Sb film, approaching a limiting thickness of about 2.5 ML Sb. Assuming this thickness as the Sb contribution to the reacted interface and an Au contribution of about 6 ML, the limiting thickness of the amorphous layer can be estimated to be of the order of 2.3 nm.

It has to be pointed out that, at the early stage of the interface reaction, there exists a remarkable difference between the valence-band spectra of the interface layer and those of the corresponding amorphous alloys. Taking an Au coverage of, e.g., 0.5 ML, which according to Fig. 6 corresponds to an $Au_{34}Sb_{66}$ layer with thickness $D \approx 0.6$ nm, a steplike intensity at the Fermi energy would be expected as compared to the amorphous alloys. However, no indications have been found for such a steplike intensity, but only a band shape showing a monotonic decrease toward E_F, where the intensity has dropped to zero. This behavior cannot be explained as resulting from the amorphous Sb band shape superimposed by a small contribution of the reacted phase. At the Fermi energy, corresponding to a kinetic energy of 21.2 eV, the inelastic mean free path of the photoelectrons takes a value of 2.5 ML,[27] which is of the same order of magnitude as the estimated interlayer thickness. Therefore significant contributions from the semiconducting Sb substrate to the valence-band spectrum can be excluded for a homogeneously reacted interface layer where lateral discontinuities are absent. Assuming the presence of intermixed islands on top of the Sb film, i.e., assuming the reacted layer to be noncontinuous on a larger length scale, the superposition of the corresponding spectra should result into a reduced but nonzero density of states at E_F which is not observed in Fig. 1.

The reason for the discrepancy mentioned above may be found in the details of the Sb surface which is believed to exhibit a certain roughness. Using an amorphous semiconductor as a substrate film, ultrathin metallic layers can usually be prepared at low temperatures showing a finite conductance even in the submonolayer range [e.g., Pb or Bi deposited on Ge at 4 K (Ref. 2)]. By analyzing the conductance as a function of the metal overlayer thickness, percolation in two dimensions has been reported to play an important role in the explanation of the onset of conductivity. Percolation, however, relates the onset of conductivity (corresponding to a critical coverage) to the development of a network of conducting paths where charge can flow over macroscopic distances. These conducting paths, which, for $D_{Au}=0.5$ ML, are due to an intermixed $Au_{34}Sb_{66}$ phase, should behave, in the simplest picture, like one-dimensional metallic systems with a vanishing density of states at the Fermi energy. Well beyond the critical value, the current will flow through a two-dimensional and, for higher coverages, a three-dimensional metallic material corresponding to a steplike density of occupied electronic states at the Fermi energy. As will be shown below, first indications for a finite conductivity were observed at a critical overlayer thickness of $D_{Au} \leq 0.4$ ML, thus supporting the idea that at the early stage of interface formation both effects, intermixing and changing dimensionality, play an important role in the determination of the electronic structure of the reacted layer. However, a detailed morphological study will be needed in order to get a better understanding of this problem.

B. Core-level spectroscopy on Au/Sb bilayers

By examining the changes of the substrate and adsorbate core levels during the interlayer growth it is possible to deduce additional chemical and structural information about the various stages of interface formation. Core-level binding energies and line shapes are intimately related to the local chemical environment of the probed atoms. Changes in the valence-band structure due to bonding are usually reflected in ground-state binding-energy shifts of core electrons with respect to the pure material. On the other hand, relaxation and screening of the photoionized core hole state by valence electrons are also known to contribute to the measured binding-energy shifts[28] as well as to influence the core-level line shapes.[29]

Core-level spectra of both the Sb substrate (Sb $3d$) and the Au toplayer (Au $4f$) were examined in greater detail to evaluate the nature of the overlayer growth mode. All core-level spectra were analyzed applying a numerical least-squares-fitting procedure[30] using Doniach-Sunjic (DS) line shapes.[29] Briefly, the DS model function results from the convolution of a Lorentzian with a one-sided power law with singularity index α. The Lorentzian reflects the lifetime width of the photoionized core hole state and the singularity index α manifests the effects of the screening response of the valence electrons. This parameter can be correlated with the local density of states at the Fermi energy.[31] To allow a comparison to measured photoemission data, the DS line shape has to be convoluted with a Gaussian, representing the combined effects of instrumental resolution, phonon excitation, and, as we will see below, other sources of broadening.

The Au $4f$ spectrum presented in Fig. 7 has been acquired after the evaporation of 1 ML of Au on top of

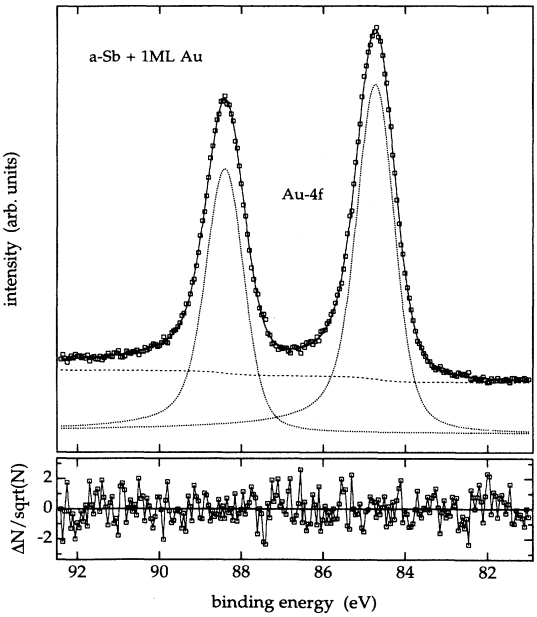

FIG. 7. MXPS photoemission spectrum of the Au/Sb overlayer system ($D_{Au}=1$ ML) showing the Au $4f$ core-level region. The squares are data points measured at a photon energy of 1486.6 eV ($T=77$ K). The full line indicates the result of a least-squares fit using two Doniach-Sunjic lines (dotted curves) and an integral background (dashed line). The residuals, i.e., the normalized difference between the data and the fitted core lines, are shown in the bottom panel.

amorphous Sb. The data have been fitted with a spin-orbit doublet having a DS line shape. The residuals (lower part of Fig. 7) indicate that no additional component has to be added to give a reasonable quality of the fit. The resulting line-shape parameters are summarized in Table I together with data obtained for higher Au coverages. At the early stage of Au deposition where, according to the UPS results, an intermixed layer will form ($D_{Au} \leq 6$ ML), a single spin-orbit doublet has been found to be sufficient to describe the core-level spectra. In this range of the overlayer thickness a strongly increased Gaussian width can be recognized which is larger than that expected on the basis of the instrumental broadening (≈ 0.6 eV). This suggests an additional broadening due to a large number of inequivalent sites around the probed Au atoms since phonon broadening is unlikely to occur at 77 K. The singularity index of about 0.06 is significantly larger than that of bulk Au, i.e., the photoionized Au $4f$ core hole in the interface layer is much better screened than an Au $4f$ core hole in pure Au. This gives direct evidence for the existence of additional Sb derived states at the Fermi energy, which must be strongly hybridized with the Au $6s$ electrons to increase the local density of conduction electrons around the probed Au atoms. This result confirms the conclusion of a chemical reaction between the adsorbed Au atoms and the Sb substrate at 77 K.

TABLE I. Au $4f_{7/2}$. An asterisk denotes fitted with an additional component due to a surface core-level shift. Parameters refer to the main line.

D_{Au} (ML)	Singularity index α	Lifetime width (eV)	Gaussian width (eV)	E_b (eV)
1	0.057	0.329	0.879	0.567
3	0.061	0.303	0.844	0.397
6	0.059	0.295	0.772	0.116
25*	0.026	0.314	0.613	0.063
75*	0.026	0.281	0.654	−0.033
bulk*	0.026	0.273	0.630	0

In the case of the very thick overlayers (e.g., $D_{Au}=25$ ML), the experimental data could not be adequately fitted with less than two components: a surface shifted component[32] had to be added to the main lines comparable in strength and binding energy with the values obtained for the surface contribution to the reference sample data (not shown here). In addition, the line-shape parameters of the main lines identify the corresponding core-level spectra as being due to polycrystalline Au. Such a result will be expected on the basis of an unreacted pure Au layer with thickness $D_{Au}=19$ ML located on top of an amorphous intermixed layer by taking into account that the inelastic mean free path of the Au $4f$ photoelectrons is about 8 ML.[27]

Unfortunately, such a line-shape analysis could not be performed with the earlier results on amorphous Au_xSb_{100-x} alloys because in those experiments no monochromatized x-ray source had been available. Rather those data were obtained with a standard source (Mg $K\alpha, h\nu=1253.6$ eV) allowing less energy resolution. However, these earlier XPS results can be used to determine approximate values for the core-level binding energies. In Fig. 8 Au $4f$ binding-energy shifts as compared

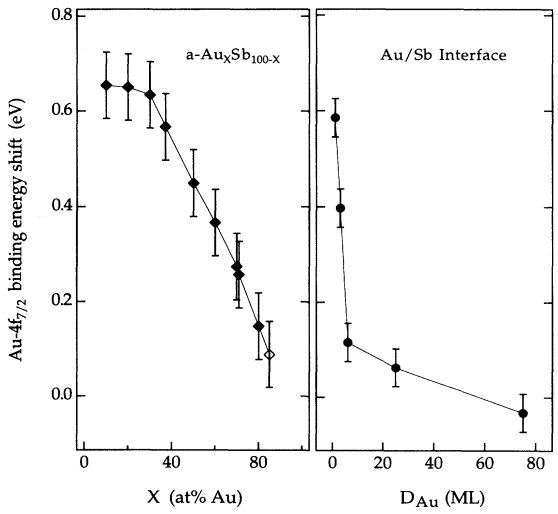

FIG. 8. Au $4f$ binding-energy shifts as compared to pure Au for the amorphous Au_xSb_{100-x} alloys (left panel, full squares) and the reacted interlayer (right panel, full dots), respectively. Full lines are given as a guide to the eye. The open square refers to the binding-energy shift measured on $Au_{85}Sb_{15}$, which is assumed to be partly crystallized.

to pure Au are shown for the amorphous Au_xSb_{100-x} alloys and for the Au/Sb interface, respectively. For the lowest Au content in the alloy ($x=10$) a large shift to higher binding-energy values (0.65 eV) occurs, which is constant for compositions up to 30 at. % Au. At higher-x values a rapid decrease is observed approaching a value of 0.15 eV at the limiting concentration where an amorphous phase can exist ($x=80$). According to the interpretation of the UPS spectra it is a natural conjecture that for the chemically reacted amorphous interlayer similar binding-energy shifts should occur as for the corresponding amorphous films. This is exactly what can be seen in the right panel of Fig. 8. For 1 ML of Au on top of Sb the average Au concentration of the reacted interface layer is estimated to be about 43 at. % (see Fig. 6). In this case, intermixing at the interface leads to a measured binding-energy shift of 0.57 eV, which, within the error bars, compares very well with the shift estimated for the corresponding amorphous $Au_{34}Sb_{57}$ alloy (0.51 eV). After increasing the number of Au atoms up to an overlayer thickness of 6 ML, the Au $4f$ binding-energy shift drastically flattens towards a value of 0.12 eV, which, within the error bars, coincides with the value of 0.09 eV measured for $Au_{85}Sb_{15}$. The distinct change in slope at a coverage of 6 ML indicates the development of a new growth mode.

The large Au $4f$ core-level binding-energy shifts apparent for the amorphous alloys (0.65 eV) and the chemically reacted interface layer ($D_{Au}=1$ ML, 0.57 eV) have to be studied in more detail in order to separate the ground-state contribution from the shift which will be caused by final-state relaxation and screening effects. This analysis can be done within the thermodynamic model which has been developed by Johansson and Mårtensson.[33] This model has proved to be a very successful description for crystalline,[28] liquid,[34] and amorphous[35] alloys as well as clusters supported on different substrates.[36] Within this model the resulting binding-energy shift, if an atom A is removed from the pure metal and dissolved in host B, can be expressed as

$$\Delta E_b = E(A;B) - E(A+1;B) + E(A+1;A) . \quad (1)$$

The term $E(A;B)$ represents the enthalpy of solution at infinite dilution of atom A in host B and the term $A+1$ refers to an atom with atomic number one greater than that of A. While the first term reflects the ground-state binding-energy shift upon solution, the other two terms reflect the response of the conduction electrons to the photoionized core hole. Using calculated heats of solution which can be taken from the semiempirical scheme of Miedema and co-workers[37,38] the above formula may be taken as a first approximation to deduce the binding-energy shift originating from the solution of up to 30 at. % of Au into Sb. This seems to be reasonable because of the saturation behavior observed for the Au $4f$ binding energy for alloy concentrations $x \leq 30$ (see Fig. 8). The application of the above model yields an estimated binding-energy shift of 0.57 eV, which agrees fairly well with the values measured for the amorphous alloys and the intermixed layer. Consequently, the large core-level

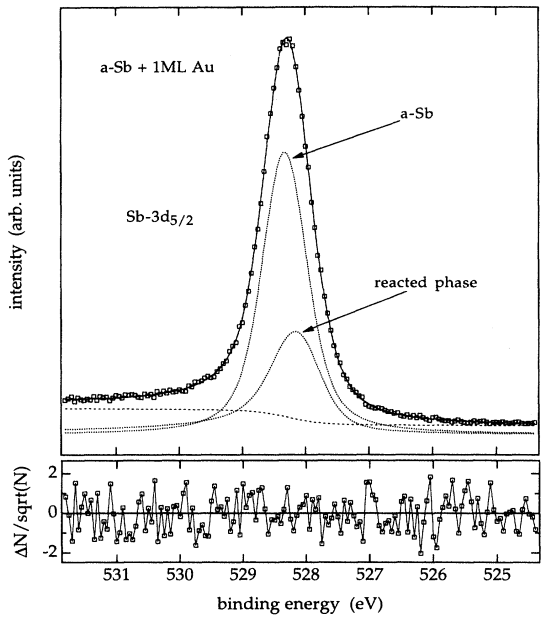

FIG. 9. Least-squares analysis of the Sb $3d_{5/2}$ core line of the overlayer system introduced in Fig. 7 ($D_{Au}=1$ ML). The data have been fitted with two lines corresponding to the disordered Sb substrate (fixed line-shape parameters) and the chemically reacted phase (parameters free adjustable).

shifts can be discussed as being due to a ground-state shift of 0.32 eV superimposed by a final-state contribution of 0.25 eV. The ground-state shift to higher binding energies, as observed for the reacted interlayer, therefore reflects an energy gain of the system at 77 K even though an amorphous rather than a crystalline compound has been formed.

In Fig. 9 photoemission data are presented for the substrate Sb $3d_{5/2}$ core level that have been acquired after deposition of 1 ML Au. Because of an inelastic mean free path of 6.5 ML for the Sb $3d$ photoelectrons[27] and an estimated interface layer thickness of about 3 ML (1 ML Au+2 ML Sb, see Fig. 6) it is reasonable to assume that the Sb $3d_{5/2}$ line can be modeled as the sum of two components originating from the pure Sb substrate and the intermixed phase, respectively. In order to get a reasonable quality of the fit, the Sb $3d_{5/2}$ line had to be superimposed by the tail of the Sb $3d_{3/2}$ level and an additional component reflecting the existence of a small O $1s$ signal at $E_b=533.4$ eV. The resulting line-shape parameters are summarized in Table II.

In the disordered state at 77 K the Sb core levels reveal a singularity index $\alpha \equiv 0$, which is equivalent to a vanishing density of states near the Fermi energy, consistent with the UPS data presented in Fig. 1. In the crystalline state the Sb $3d$ levels are characterized by an asymmetry parameter α comparable with that of the Au reference sample. After the deposition of Au atoms on top of a-Sb, the singularity index α corresponding to the reacted phase drastically increases to a value of about 0.1. This gives clear evidence that now electronic states at the Fer-

TABLE II. Sb $3d_{5/2}$. An asterisk denotes fitted with two components representing the substate (*a*-Sb) and the interface layer contribution to the core-level spectrum, respectively. Parameters refer to the intermixed phase.

D_{Au} (ML)	Singularity index α	Lifetime width (eV)	Gaussian width (eV)	E_b (eV)
c-Sb	0.029	0.436	0.604	0.028
a-Sb	0.000	0.432	0.587	0
1*	0.115	0.401	0.647	−0.216
3*	0.101	0.435	0.678	−0.052
6*	0.111	0.413	0.670	−0.100

mi level are present at Sb sites screening the positively charged hole state during the photoemission process. These electronic states, which are absent in pure disordered Sb, must be generated even at low temperature by chemical reactions between the Au atoms and those Sb atoms which are located at the surface of the substrate film.

Similar chemical reactions have been reported to occur for an Sb overlayer ($D_{Sb} \approx 0.5$ ML) adsorbed on an Au single crystal at room temperatures.[39] At this temperature, where amorphous Au_xSb_{100-x} alloys are no longer stable,[12,26] a singularity index of 0.08 has been extracted for the Sb 4*d* core levels by means of synchrotron radiation-induced photoemission which allows a better energy resolution as compared to our experiment. From the similarity of both values it can be concluded that the strength of the chemical reactions occurring at Au/Sb interfaces does not strongly depend on temperature, in contrast to the structure (ordered or disordered) of the resulting intermixed phase.

The binding-energy shifts of the Sb 3*d* levels, extracted by the fitting procedure, are significantly smaller than the corresponding values of the Au 4*f* levels. Unfortunately theoretical binding-energy shifts according to the thermodynamic model are not available because of missing values for some of the enthalpies of solution, necessary to apply formula (1). In addition, a more precise analysis of the Sb 3*d* core-level shifts with respect to the amorphous films is not possible because of too large scatter in both sets of data. However, both systems reveal binding-energy shifts of the same order of magnitude (≈ -0.1 eV).

In summary, the core-level spectroscopy measurements are found to be consistent with the conclusions which have been drawn from the UPS results. As indicated by a significantly enhanced asymmetry of the core lines, chemical reactions must occur between the different types of atoms at Au/Sb interfaces, leading to the formation of an alloy with a disordered structure as long as the deposition of Au atoms does not exceed a critical thickness of about 6 ML. These findings, which have been extracted from experiments on Au/Sb bilayers, will now be employed to understand the properties of Au/Sb multilayers.

C. Resistance measurements on Au/Sb multilayers

As in the previous case of spectroscopic data, the resistance behavior during the deposition of Au atoms at $T_s = 130$ K on top of Sb has been studied first for "thick" bilayers (15-nm-thick Sb and 4.2-nm-thick Au). Typical results are shown in Fig. 10, where the resistances as observed during the deposition of the different atomic species are plotted versus the film thickness. Figure 10(a) gives an enlarged view of the Sb growth on top of an Au film, the preparation of which resulted in an almost linear resistance decrease on the scale of this figure, as can be seen to the left of the arrow indicating the start of the Sb deposition. The arriving Sb atoms lead to a steep resistance increase for a Sb thickness of up to about 1 nm. Further Sb deposition results in a saturation of this increase at a thickness-independent resistance value, which remains constant after switching off the Sb preparation. The spectroscopic results introduced above suggest the following interpretation of these resistance data. The Sb atoms react with the topmost Au atoms to form an amorphous Au_xSb_{100-x} interface layer, which possesses a much higher electrical resistivity than the pure polycrystalline Au film, thereby leading to a resistance increase as observed. This reaction, however, is restricted to a Sb thickness of less than about 1 nm. Above this value, further Sb deposition results in an amorphous semiconducting (at 130 K insulating) Sb film, which does not contribute to the experimentally determined resistance, i.e., a thickness-independent resistance value is obtained. If Au is deposited on top of this amorphous Sb film, resistance changes are observed as presented in Fig. 10(b), again on an enlarged thickness scale. There the left arrow indicates the start of Au deposition; at the right arrow this

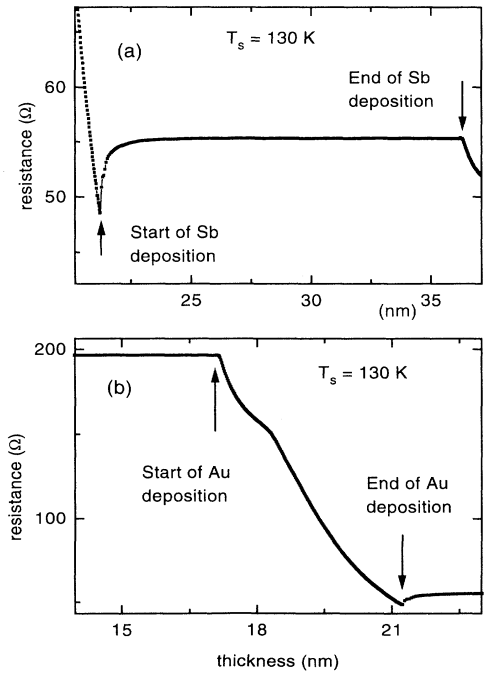

FIG. 10. Electrical resistance during the preparation of a Au/Sb bilayer at $T_s = 130$ K with individual layer thicknesses of 4.2 nm for Au and 15 nm for Sb as a function of the film thickness (a) during Sb-layer preparation and (b) during Au-layer preparation.

deposition is stopped. Clearly, the Au atoms on top of Sb lead to a strong resistance decrease, which exhibits a significant structure. For the first 1.5 nm of Au corresponding to about 6 ML, a very steep resistance drop is observed, which flattens out and is followed by the typical hyperbolic dependence as expected for pure polycrystalline Au films. Again, the anomalous initial resistance decrease seen for the first 1.5 nm of Au can be explained by assuming an interface reaction of the Au atoms with the topmost Sb atoms forming an amorphous metallic interlayer followed by the growth of a highly conducting polycrystalline Au film. It is worth noting that the drastic resistance decrease can be observed even for Au thicknesses below 0.1 nm, for which percolating paths of *pure* Au can be excluded, supporting the idea of an interface reaction.

Thus both the spectroscopic as well as the resistivity results indicate an interface reaction for the Au/Sb system, leading to the formation of an amorphous interlayer under the above conditions, which is restricted to below a critical thickness. As a consequence, if the individual Au and Sb layers are kept below their critical thicknesses, the interface reaction should be complete and result in an homogeneous amorphous layer. Furthermore, by stacking such "subcritical" bilayers, a homogeneous, thick, amorphous film should be obtained. The resistance behavior during the preparation of such a multilayer system is shown in Fig. 11 on an enlarged thickness scale. In this case, an Au/Sb multilayer with individual thicknesses of 0.42 nm of Au and 1.5 nm of Sb were periodically topped on each other at $T_s = 130$ K up to a total thickness of about 40 nm. Assuming complete interface reactions, the above thickness ratio corresponds to a nominal resulting composition of $AuSb_2$. The observed periodic resistance behavior reflects the expected interface reactions, as already explained in the context of Fig. 10. Together with the independently determined film thicknesses, the resistivity of each completely reacted bilayer can be calculated giving a value of 145 $\mu\Omega$ cm, in good agreement with the corresponding result obtained for quench-condensed amorphous $AuSb_2$ films.[12,26] This confirms that an amorphous rather than a polycrystalline interface alloy is formed by the observed reaction. A critical final test of this conclusion is provided by an annealing experiment of the multilayer system. If a homogeneous amorphous film has been formed by successive complete interface reactions, a well-defined crystallization temperature T_x characterized by a narrow irreversible resistance drop should be observed on annealing. The corresponding result of such an experiment is presented in Fig. 12, where the resistivity of the multilayer system from Fig. 11 is plotted versus the annealing temperature during continuous heating at a rate of 1 K/min up to a maximum of 390 K. Three characteristic temperature regimes can be distinguished: Up to $T_x = 285$ K only a slight irreversible resistivity decrease is observed and the film exhibits a negative reversible temperature coefficient $d\rho/dT = -0.053$ $\mu\Omega$ cm/K, as determined by recooling at 180 K (indicated by a double arrow in Fig. 12). Such a negative $d\rho/dT$ value is typical of amorphous metals. At T_x, an irreversible narrow resistivity drop occurs, reflecting the crystallization of the amorphous phase followed by a broad, further decrease, indicating annealing and grain growth of the polycrystalline phase. By recooling from 390 K a typical metallic reversible behavior is found with $d\rho/dT = +0.038$ $\mu\Omega$ cm/K. The x-ray-diffraction pattern of this crystalline metallic alloy revealed only lines of the cubic $AuSb_2$ structure, confirming a complete reaction of the multilayers in accordance with the Au/Sb thickness ratio. The obtained value of $T_x = 285$ K is again in good agreement with the crystallization temperature of amorphous $AuSb_2$ films.[12,26] Thus this result completes the experimental proof that an amorphous interlayer of restricted thickness is formed at Au/Sb interfaces even at low temperatures.

Once an amorphous interlayer has been formed by the reaction, it will be stable up to T_x. The question arises, however, of whether T_x is identical to the upper limit of

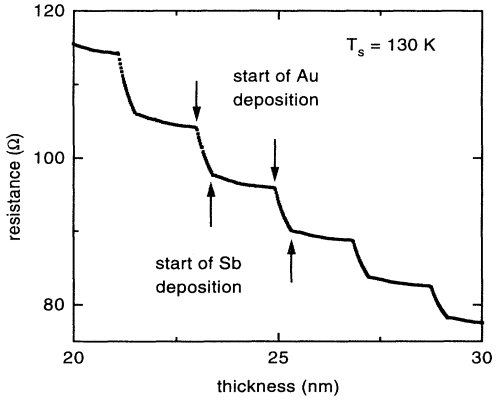

FIG. 11. Electrical resistance as observed during the preparation at $T_s = 130$ K of the multilayer $20\times$(0.42-nm-thick Au + 1.5-nm-thick Sb) versus total film thickness on an enlarged scale showing the deposition of only five bilayers. The arrows indicate the start and stop of Au and Sb deposition, respectively.

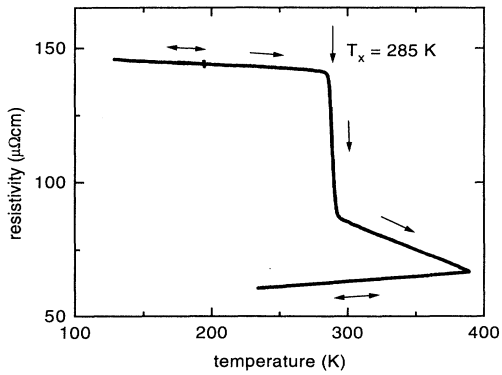

FIG. 12. Post-deposition annealing behavior of the resistivity of the Au/Sb multilayer introduced in Fig. 11. Irreversible resistance changes are indicated by arrows, reversible changes by double arrows.

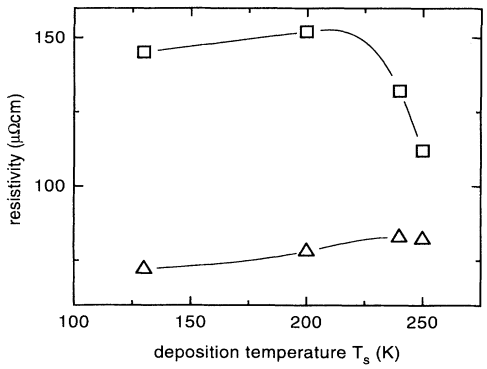

FIG. 13. As-prepared resistivities of Au/Sb multilayers with an average composition $AuSb_2$ versus deposition temperature T_s (open squares). Triangles denote resistivities of the same layers at T_s after annealing up to 330 K.

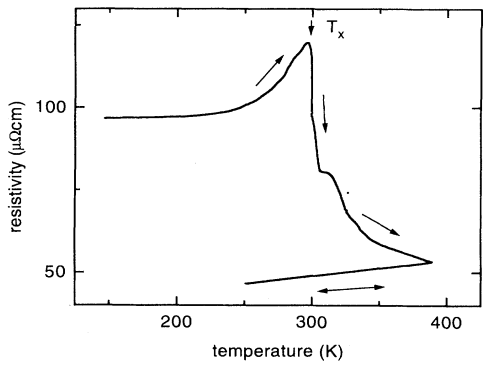

FIG. 14. Resistivity changes of a "thick" double Au/Sb bilayer 2×(15-nm-thick Sb + 4.2-nm-thick Au) due to thermal annealing.

deposition temperatures T_s for which the amorphous, rather than a crystalline phase is obtained due to kinetic constraints. This question is answered by the results shown in Fig. 13. Here the as-prepared resistivity values of the same type of multilayers as in Fig. 11 (0.42 nm of Au and 1.5 nm of Sb, total thickness 40 nm) are plotted as a function of various deposition temperatures T_s (open squares) together with corresponding data obtained after annealing the systems up to 330 K $> T_x$ and recooling to T_s (open triangles). Clearly, up to 200 K the as-prepared resistivities remain constant, indicating complete amorphization by the interface reactions. For higher-T_s values a significant resistivity decrease is observed approaching the crystalline behavior. Furthermore, the multilayers prepared at 250 K no longer exhibit a resistance drop at T_x; rather they approach the crystalline value over a broad temperature range. This observation suggests that the kinetic constraints necessary to obtain amorphous layers by interface reactions are lifted for $T_s > 240$ K and, as a result, crystalline alloys are formed even below T_x. The physical reason for this can be better understood and related to the onset of long-range interdiffusion by studying thick Au/Sb bilayers (4.2 nm of Au and 15 nm of Sb, as in Fig. 10) prepared at 130 K. From the data presented so far, it is clear that these as-prepared bilayers consist of an amorphous interlayer sandwiched by still unreacted Au and Sb films, respectively. Electrically, since the unreacted Sb film is insulating, the total resistance is dominated by the unreacted Au. Thus, depending in detail on the different thicknesses, the resulting resistivity in all cases is lower than for a completely amorphous layer. A corresponding experimental example is given in Fig. 14, where the resistivity of two such bilayers on top of each other is plotted as a function of the annealing temperature. Up to about 230 K the resistivity remains practically constant at the as-prepared value of 96 $\mu\Omega$ cm, which is as expected, significantly lower than for a completely amorphous film. At 230 K, the resistivity starts to increase, approaching a value of 120 $\mu\Omega$ cm at 290 K, followed by the steep irreversible resistivity drop at 295 K due to the crystallization of the amorphous interlayers. Above this temperature, further annealing over a broad temperature regime is observed and by recooling from 390 K, the reversible (double arrow) resistivity behavior is obtained, typical of a crystalline metallic alloy. An important feature in this figure is the resistivity increase starting at 230 K, which indicates the onset of further Au and Sb interdiffusion. This interdiffusion, however, cannot lead into the amorphous phase, as has been shown in the context of Fig. 13, since above 240 K only crystalline though still disordered phases are formed. Thus the picture arises that for $T_s > 240$ K the kinetic constraints necessary for amorphization by interface reactions are lifted by the occurrence of long-range interdiffusion even though the amorphous phase is still stable at this temperatures if prepared well below.

It is worth noting that a series of Au/Sb multilayers have been prepared at 130 K with varying layer thickness ratios spanning a wide range of nominal compositions in the case of complete interface reactions from $Au_{70}Sb_{30}$ to $Au_{30}Sb_{70}$. In all cases, amorphous interlayers were obtained with as-prepared resistivities and crystallization temperatures T_x, in good agreement with the corresponding results of quench-condensed amorphous films.[12,26]

As outlined above, clear experimental evidence has been found for the formation of an intermixed layer of restricted thickness at Au/Sb interfaces even at low temperature. The structure of this interlayer could be identified as being amorphous by means of different analytical methods, yielding this result with a high degree of consistency. In order to understand the underlying growth processes in more detail, a microscopic picture would be helpful in describing, for example, the adhesion of Au atoms on a Sb surface at low temperature. It has been demonstrated that thermally activated long-range interdiffusion can be excluded as being responsible for these amorphization processes. Based on the observed strong similarities of the interlayer results to the properties of quench-condensed amorphous alloys, a simple physical picture will be proposed which may be taken as a first approximation for the underlying effects as long as detailed theoretical and experimental investigations are

absent.

During the past decade amorphous alloys of the noble-metal–polyvalent-element type have been the subject of intense research (for a review, see Ref. 25). In these materials, which can uniquely be described in terms of amorphous Hume-Rothery alloys, the conduction electrons usually show a similar strong influence on the atomic structure as in the crystalline case. On the other hand, it has been demonstrated that there also exists a strong influence of the disordered atomic structure on the conduction electrons, resulting in a minimum or pseudogap in the density of states at the Fermi level, as originally proposed by Nagel and Tauc in 1975.[40] The existence of such a pseudogap (which is equivalent to a lowering of the total energy of the electronic system as compared to a free-electron model) has been argued to be responsible for the forming ability as well as for the stability of this type of alloy against crystallization. Within a modern interpretation, such a pseudogap can be understood as being due to the screening of the ions by the nearly free *sp* electrons giving rise to charge-density oscillations around the ions leading to Friedel oscillations in the effective pair potential. These oscillations are responsible for the observation of strong medium-range order in the positions of the ions (i.e., the atoms tend to reside at positions corresponding to minima in the oscillating pair potential), resulting in a shoulder or a peak in the structure factor $S(q)$ at wave numbers $q \approx 2k_F$, with $2k_F$ the diameter of the smeared-out Fermi sphere. As a consequence, *sp* electrons with Fermi momentum are forced to enhanced umklapp scattering from the amorphous structure, leading to a pseudogap in the density of states at E_F.

Assuming that this description also holds true for the amorphous interlayer, a pseudogap will be expected at the Fermi level during the layer growth. This is exactly what can be seen in Fig. 15 for the occupied part of the valence band. Here the low-binding-energy range has been plotted for an intermixed layer ($D_{Au}=3$ ML) and the corresponding amorphous alloy ($Au_{60}Sb_{40}$). In both cases, a significant decrease of the density-of-states curves toward the Fermi energy is obvious, which is even more pronounced for the intermixed phase. Therefore the following picture emerges about the growth of the interlayer. When Au atoms are deposited onto a clean, insulating Sb substrate, the 6*s* electrons of Au interact with the valence-band electrons of Sb to form hybridized states. This hybridization results in local changes of the electron density and is accompanied by structural relaxations of the Au and Sb atoms on a length scale which, because of strong kinetic constraints at low temperature, corresponds to the nearest-neighbor distance. As shown by Hafner and co-workers,[41,42] this feedback process between local atomic arrangements and local electronic structure has to be treated self-consistently. It can be described by adjusting the atomic positions to the minima of a screened effective pair potential, which, in turn, can be characterized by the wavelength of the Friedel oscillations and this wavelength, on the other hand, is determined by the local electron density. The feedback loop is closed by the dependence of the electronic density on the atomic arrangement. After having obtained the metallic state, this feedback mechanism results in the pseudogap described above, the experimental evidence of which has been presented in Fig. 15 for the disordered Au/Sb system. Adding more and more Au atoms to the metallic state leads to a continuous lowering of the average electron density toward a value of 1.8 electrons per atom (corresponding to $Au_{80}Sb_{20}$), which is known to be a limiting value for the formation of amorphous Hume-Rothery alloys.[25]

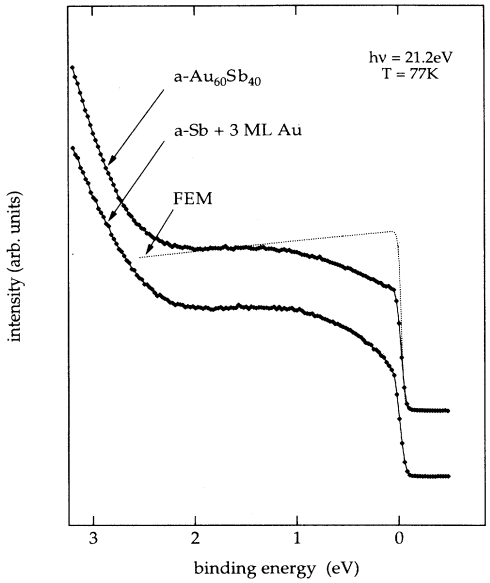

FIG. 15. Valence-band spectra ($h\nu=21.2$ eV) of the intermixed phase ($D_{Au}=3$ ML) and the corresponding vapor-quenched amorphous $Au_{60}Sb_{40}$ alloy on an enlarged scale, showing a strong decrease of the density of states toward the Fermi energy E_F. All experimental data have been corrected for satellite and secondary-electron contributions as well as for the transmission function of the energy analyzer. In order to demonstrate the strength of the pseudogap, a density-of-states curve has been added (dotted line) which was calculated for $Au_{60}Sb_{40}$ within a free-electron model (FEM).

IV. CONCLUSION

In conclusion, photoelectron spectroscopic methods combined with resistance measurements have proved to be a valuable tool in order to characterize the intermixing processes which occur at Au/Sb interfaces even at low temperatures. Strong experimental evidence has been found for the formation of an amorphous intermixed layer of restricted thickness, which cannot be explained on the basis of thermally activated long-range interdiffusion, but rather within a model demonstrating the importance of correlation effects between the electronic and atomic structure of the intermixed phase. Taking advantage of this amorphization reaction, thick amorphous samples could be obtained with properties similar to those of quench-condensed amorphous films.

ACKNOWLEDGMENTS

We thank T. Koch for valuable discussions and experimental assistance. The continuous financial support by Schweizer Nationalfonds and Deutsche Forschungsgemeinschaft within SFB 306 is gratefully acknowledged.

---

*Present address: Institut für Physik, TU Chemnitz-Zwickau, D-09107 Chemnitz, Germany.

[1]N. Cherradi, A. Audouard, A. Kazoun, and G. Marchal, Solid State Commun. **70**, 315 (1989).
[2]D. B. Haviland, Y. Liu, and A. M. Goldman, Phys. Rev. Lett. **62**, 2180 (1989).
[3]H. M. Jaeger, D. B. Haviland, A. M. Goldman, and B. G. Orr, Phys. Rev. B **34**, 4920 (1986).
[4]L. M. Falicov, Phys. Today **45** (10), 46 (1992).
[5]R. E. Camley and R. L. Stamps, J. Phys. Condens. Matter **5**, 3727 (1993).
[6]G. Bergmann, Phys. Rev. B **36**, 11 280 (1989).
[7]E. Compans and G. Bergmann, Z. Phys. B **79**, 203 (1990).
[8]N. Giordano and N. R. Dilley, Phys. Rev. B **48**, 4675 (1993).
[9]A. L. Wachs, A. P. Shapiro, T. C. Hsieh, and T. C. Chiang, Phys. Rev. B **33**, 1460 (1986).
[10]M. Jalochowski, H. Knoppe, G. Lilienkamp, and E. Bauer, Phys. Rev. B **46**, 4693 (1992).
[11]J. E. Ortega, F. J. Himpsel, G. J. Mankey, and R. F. Willis, J. Phys. Condens. Matter **5**, A189 (1993).
[12]P. Häussler, W. H. G. Müller, and F. Baumann, Z. Phys. B **35**, 67 (1979).
[13]M. Seyffert, A. Siber, and P. Ziemann, Phys. Rev. Lett. **67**, 3792 (1991).
[14]A. Siber, J. Marien, T. Koch, and P. Ziemann, Appl. Phys. A **57**, 267 (1993).
[15]W. L. Johnson, Prog. Mater. Sci. **30**, 81 (1986).
[16]K. Samwer, Phys. Rep. **161**, 1 (1988).
[17]B. M. Clemens, Phys. Rev. B **33**, 7615 (1986).
[18]J. Y. Cheng and L. J. Chen, J. Appl. Phys. **69**, 2161 (1991).
[19]B. Blanpain, L. H. Allen, J.-M. Legresy, and J. W. Mayer, Phys. Rev. B **39**, 13 067 (1989).
[20]R. Fink, T. Koch, G. Krausch, J. Marien, A. Plewnia, B.-U. Runge, G. Schatz, A. Siber, and P. Ziemann, Phys. Rev. B **47**, 10 048 (1993).
[21]T. Koch, A. Siber, J. Marien, and P. Ziemann, Phys. Rev. B **49**, 1996 (1994).
[22]R. G. Zhao, Y. Zhang, and W. S. Yang, Phys. Rev. B **48**, 8462 (1993).
[23]M. Seyffert, A. Siber, and P. Ziemann, Thin Solid Films **208**, 197 (1992).
[24]J. Yeh and I. Lindau, At. Data Nucl. Data Tables **32**, 1 (1985).
[25]P. Häussler, Phys. Rep. **222**, 65 (1992).
[26]C. Lauinger, Ph.D. thesis, University of Karlsruhe, 1993.
[27]M. P. Seah and W. A. Dench, Surf. Interface Anal. **1**, 1 (1979).
[28]P. Steiner, S. Hüfner, N. Mårtensson, and B. Johansson, Solid State Commun. **37**, 73 (1981).
[29]S. Doniach and M. Sunjic, J. Phys. C **3**, 385 (1970).
[30]G. K. Wertheim and S. B. Dicenzo, J. Electron Spectrosc. **37**, 57 (1985).
[31]G. K. Wertheim and P. H. Citrin, Topics Appl. Phys. **26**, 197 (1978).
[32]P. H. Citrin, G. K. Wertheim, and Y. Baer, Phys. Rev. B **27**, 3160 (1983).
[33]B. Johansson and N. Mårtensson, Phys. Rev. B **21**, 4427 (1980).
[34]M. Dürrwächter, G. Indlekofer, H.-G. Boyen, P. Oelhafen, and D. Quitmann, J. Non-Cryst. Solids **156-158**, 241 (1993).
[35]H.-G. Boyen, G. Indlekofer, P. Oelhafen, M. Dürrwächter, P. Häussler, and F. Baumann, J. Non-Cryst. Solids **156-158**, 263 (1993).
[36]M. G. Mason, Phys. Rev. B **27**, 748 (1983).
[37]A. R. Miedema, P. F. d. Châtel, and F. R. d. Boer, Physica B **100**, 1 (1980).
[38]A. K. Niessen, F. R. d. Boer, R. Boom, P. F. d. Châtel, W. C. M. Mattens, and A. R. Miedema, CALPHAD **7**, 51 (1983).
[39]G. K. Wertheim, J. E. Rowe, D. N. E. Buchanan, H. L. Polite, and H. Shigekawa, Phys. Rev. B **38**, 9606 (1988).
[40]S. R. Nagel and J. Tauc, Phys. Rev. Lett. **35**, 380 (1975).
[41]J. Hafner and M. C. Payne, J. Phys. Condens. Matter **2**, 221 (1990).
[42]W. Jank and J. Hafner, Phys. Rev. B **41**, 1497 (1990).